Spectrochimica Acta Part A: Molecular and Biomolecular Spectroscopy 131 (2014) 225–234

Contents lists available at ScienceDirect

Spectrochimica Acta Part A: Molecular and Biomolecular Spectroscopy

journal homepage: www.elsevier.com/locate/saa

Vibrational spectra, molecular structure, NBO, HOMO–LUMO and first order hyperpoalarizability analysis of 1,4-bis(4-formylphenyl)anthraquinone by density functional theory

R. Renjith [a], Y. Sheena Mary [b], Hema Tresa Varghese [b], C. Yohannan Panicker [a,*], Thies Thiemann [c,d], Christian Van Alsenoy [e]

[a] Department of Physics, TKM College of Arts and Science, Kollam, Kerala, India
[b] Department of Physics, Fatima Mata National College, Kollam, Kerala, India
[c] Graduate School of Interdisciplinary Engineering Sciences, Kyushu University, Fukuoka, Japan
[d] United Arab Emirates University, Al Ain, United Arab Emirates
[e] University of Antwerp, Chemistry Department, Universiteitsplein 1, B2610 Antwerp, Belgium

HIGHLIGHTS

- IR, Raman spectra and NBO analysis were reported.
- The wavenumbers are calculated theoretically using Gaussian09 software.
- The wavenumbers are assigned using PED analysis.
- The geometrical parameters are in agreement with that of similar derivatives.

GRAPHICAL ABSTRACT

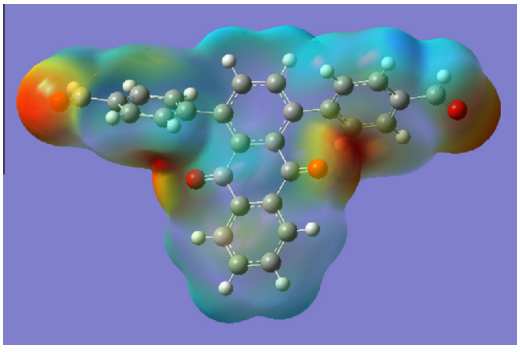

ARTICLE INFO

Article history:
Received 10 February 2014
Received in revised form 7 April 2014
Accepted 17 April 2014
Available online 26 April 2014

Keywords:
Anthraquinone
Infrared spectroscopy
Raman spectroscopy
Hyperpolarizability
DFT calculation

ABSTRACT

Anthraquinone derivatives are most important class of a system that absorb in the visible region. Infrared and Raman spectroscopic analyses were carried out on 1,4-bis(4-formylphenyl)anthraquinone. The interpretation of the spectra was aided by DFT calculations of the molecule. The vibrational wavenumbers were examined theoretically using the Gaussian09 set of quantum chemistry codes, and the normal modes were assigned by potential energy distribution (PED) calculations. A computation of the first hyperpolarizability of the compound indicates that this class of substituted anthraquinones may be a good candidate as a NLO material. Optimized geometrical parameters of the compound are in agreement with similar reported structures. The HOMO and LUMO analysis is used to determine the charge transfer within the molecule. The stability of the molecule arising from hyper-conjugative interaction and charge delocalization has been analyzed using NBO analysis.

Introduction

Anthraquinones form a group of functionally diverse aromatic compounds, structurally related to anthracene, with the parent structure being 9,10-dioxoanthracene. They are of yellow, light

* Corresponding author. Tel.: +91 9895370968.
E-mail address: cyphyp@rediffmail.com (C.Y. Panicker).

http://dx.doi.org/10.1016/j.saa.2014.04.085
1386-1425/

gray to gray-green crystalline appearance. Anthraquinones occur naturally in some plants, fungi, lichens and insects, where they serve as a basic skeleton for their pigments. Industrially, simple anthraquinones are used as precursors of dye-stuff. Dave and Ledwani [1] reported on the pharmacological properties of *Cassia* species due to the presence of anthraquinones. Anthraquinones are used as laxatives, mainly as their glycosidic derivatives, and are used in the treatment of fungal skin diseases [2]. Also, they have been found to exhibit antioxidant properties [3]. Antitumor activities of some 2-(1-aryl-1-hydroxymethyl)-, 2-aroyl-1,4-dihydroxy-9,10-anthraquinone derivatives and of 2-(1-aryl-1-hydroxymethyl)-anthracene-1,4,9,10-tetraone derivatives have been reported by Nam et al. [4]. In regard to their cytotoxicity, further studies have been carried out on the structure–activity relationship of 2-substituted-1,4-dihydroxy-9,10-anthraquinones [5,6]. Neoplastics such as mitoxantrone and pixanthrone have a 9,10-anthraquinone skeleton, while anthracyclines can be viewed as expanded 9,10-anthraquinones. In all, anthraquinones and plant extracts containing anthraquinones are being increasingly used for cosmetics, food, dye and pharmaceuticals [7]. Interestingly, some anthraquinones such as amino anthraquinones have shown third order non linear optical behaviour and some amino derivatives of anthraquinone have already been used as dyes in liquid displays [8]. Thus, a detailed understanding of the electronic properties of anthraquinones, including their possible applications in nonlinear optics (NLO), becomes more important. In general, nonlinear optics (NLO) deals with the interaction of materials with applied electromagnetic fields, altered in wavenumber, phase, or other physical properties [9], where organic molecules able to manipulate photonic signal efficiently in this way are of importance in technologies such as optical communication, optical computing, and dynamic image processing [10]. Joseph et al. [11] reported on the first hyperpolarizability of 1-(4-methoxyphenyl)-4-methylanthraquinone. The UV/Vis absorption spectra of anthraquinones solvated in methanol and ethanol have been predicted theoretically by Jacquemin et al. [12] using the time dependent DFT theory for the excited state calculations and the polarisable continuum model for evaluating bulk solvent effects. In this context, phenyl substituents can increase the hyperpolarizability of these type of molecules [13,14]. In the present work, the FT-IR and FT-Raman spectra of 1,4-bis(4-formylphenyl)anthraquinone (**3**) are reported, both experimentally and theoretically. The HOMO and LUMO analysis have been used to elucidate information regarding charge transfer within the molecule. The stability of the molecule arising from hyper-conjugative interaction and charge delocalization has been also analyzed using NBO analysis.

Experimental details

A number of synthetic routes to oligo substituted anthraquinones are known where some of these start from simpler anthraquinone precursors. A microwave-assisted copper-catalyzed Ullmann coupling to substituted anthraquinones has been forwarded by Baqi and Muller [5] Thiemann et al. [15] and Akrawi et al. [16] reported on the synthesis of arylated anthraquinones by cycloaddition of substituted halogenated thiophene S-oxides to benzoquinones and subsequent Suzuki cross-coupling reactions of the halogenated anthraquinones as key steps of the synthesis (Scheme 1). Lately, a similar strategy to arylated anthraquinones was provided with the reaction of dihydroxyanthraquinone triflates with arylboronic acids [17]. Here, the title compound was prepared by the Suzuki reaction of 4-formylphenylboronic acid (**2**) with 1,4-dichloroanthraquinone (**1**), which itself was obtained by cycloaddition of 2,5-dichlorothiophene S-oxide, prepared *in situ*, with benzoquinone [15].

A solution of 1,4-dichloroanthraquinone (245 mg, 0.89 mmol), 4-formylphenylboronic acid (**2**, 425 mg, 2.83 mmol), $Pd(PPh_3)_4$ (46 mg, 4.0×10^{-5} mol) [or $Pd(PPh_3)_2Cl_2$ (30 mg, 4×10^{-5} mol) and triphenylphosphine (30 mg, 0.11 mmol)] in a solvent mixture of DME (10 mL) and aq. Na_2CO_3 (2.32 g Na_2CO_3 in 15 mL H_2O, 6 mL) was kept at 70 °C for 18 h in an inert atmosphere. The solution was then cooled and poured into water (25 mL) and extracted with chloroform (3×15 mL). The combined organic phase was dried over anhydrous $MgSO_4$ and concentrated *in vacuo*. Column chromatography of the residue on silica gel (hexane/$CHCl_3$/ether 3:1:1) gave 1,4-bis(4-formylphenyl)anthraquinone (**3**, 167 mg, 45%) as a yellow solid; m.p. 243 °C; (Found: MH^+, 417.1130. $C_{28}H_{17}O_4$ requires MH^+, 417.1127). δ_H (270 MHz, $CDCl_3$) 7.51 (4H, d, $^3J = 8.1$ Hz), 7.60 (2H, s), 7.73–7.76 (2H, m), 8.02 (4H, d, $^3J = 8.1$ Hz), 8.06–8.09 (2H, m), 10.1 (2H, s, 2 CHO); δ_C (67.8 MHz, $CDCl_3$) 127.0 (2C, CH), 128.5 (4C, CH), 129.7 (4C, CH), 132.6 (2C, C_{quat}), 133.5 (2C, C_{quat}), 134.2 (2C, CH), 135.2 (2C, C_{quat}), 135.9 (2C, CH), 143.3 (2C, C_{quat}), 148.6 (2C, C_{quat}), 183.5 (2C, CO), 191.92 (2C, CHO); MS (FAB, 3-nitrobenzyl alcohol) *m/z* (%) 417 (MH^+) (3.4).

The FT-IR spectrum (Fig. 1) was recorded using KBr pellets on a DR/JASCO FT-IR 6300 spectrometer. The FT-Raman spectrum (Fig. 2) was obtained on a Bruker RFS 100/s, Germany. For excitation of the spectrum, the emission of Nd:YAG laser was used with an excitation wavelength of 1064 nm, a maximal power 150 mW; measurement on solid sample.

Computational details

Calculations of the title compound were carried out with Gaussian09 software [18] program using B3PW91/6-31G* and B3LYP/6-31G* basis sets to predict the molecular structure and vibrational wavenumbers. Calculations were carried out with Becke's three parameter hybrid model using the Lee–Yang–Parr correlation functional (B3LYP) method. Molecular geometries were fully optimized by Berny's optimization algorithm using redundant internal coordinates. Harmonic vibrational wavenumbers were calculated using analytic second derivatives to confirm the convergence to minima on the potential surface. Then frequency calculations were employed to confirm the structure as minimum points in energy. At the optimized structure (Fig. 3) of the examined species, no imaginary wavenumber modes were obtained, proving that a true minimum on the potential surface was found. The DFT method tends to overestimate the fundamental modes; therefore scaling factor (0.9613) has to be used for obtaining a considerably better agreement with experimental data [19]. The observed disagreement between theory and experiment could be a consequence of the anharmonicity and of the general tendency of the quantum chemical methods to overestimate the force constants at the exact equilibrium geometry. The optimized geometrical parameters (B3LYP/6-31G*) are given in Table S1 as supporting information. The assignments of the calculated wavenumbers are aided by the animation option of GAUSSVIEW program, which gives a visual presentation of the vibrational modes [20]. The potential energy distribution (PED) is calculated with the help of GAR2PED software package [21].

Results and discussion

IR and Raman spectra

The observed IR and Raman bands as well as calculated wavenumbers (scaled) and assignments are given in Table 1. The C—H vibrations of the aldehyde group are expected in the region 2871–2806 cm^{-1} [22]. In the present case these vibrations are

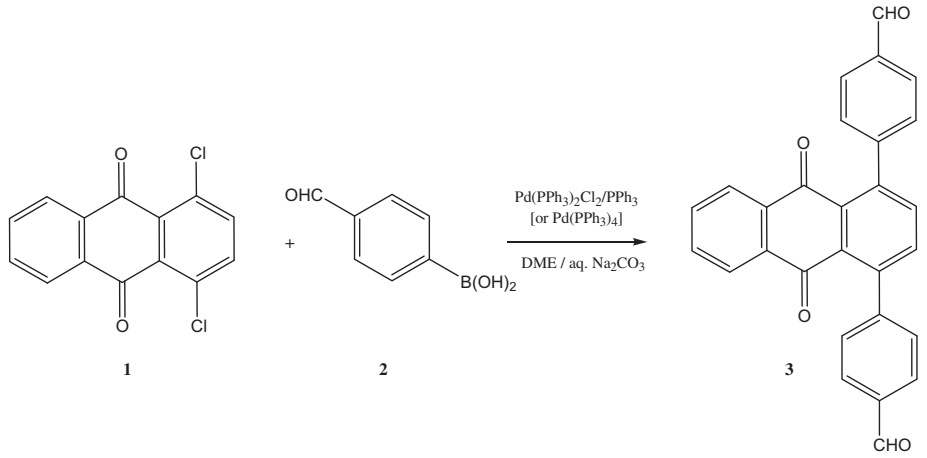

Scheme 1.

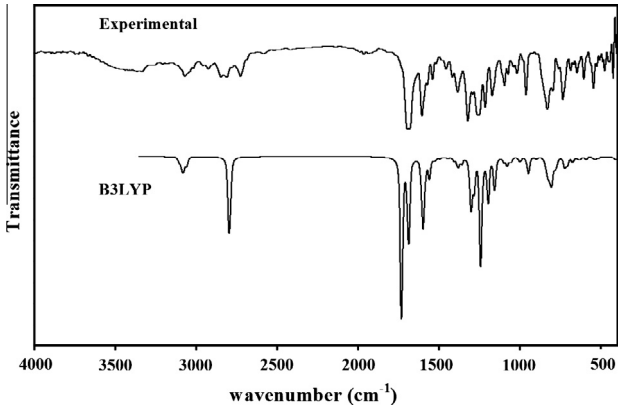

Fig. 1. FT-IR spectrum of 1,4-bis(4-formylphenyl)anthraquinone.

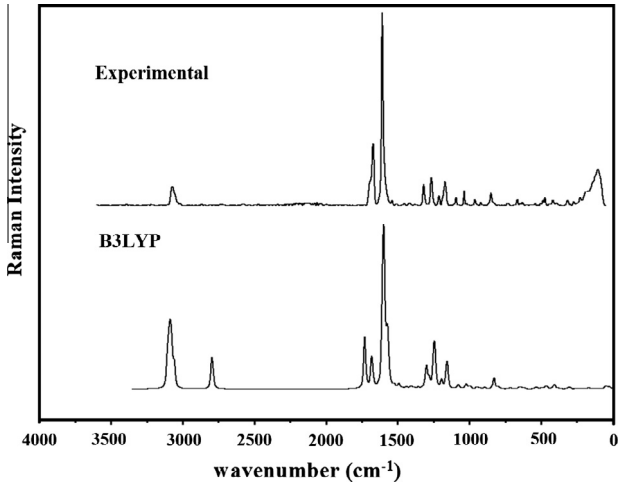

Fig. 2. FT-Raman spectrum of 1,4-bis(4-formylphenyl)anthraquinone.

assigned at 2794, 2793 cm^{-1} (B3LYP) and observed at 2725 cm^{-1} (IR) experimentally. For 5-bromo-2-methoxybenzaldehyde, Balachandran et al. [23] reported C—H stretching vibration of aldehyde group at 2898 cm^{-1} (Raman) and 2900 cm^{-1} (IR) and 2902 cm^{-1} theoretically. For the title compound the CH in-plane deformation vibrations of the aldehyde groups are assigned at 1380, 1379 cm^{-1} theoretically (B3LYP). Corresponding to this mode a medium intense band is observed at 1381 cm^{-1} in the IR spectrum. The carbonyl (C=O) stretching vibrations in the substituted benzaldehydes were reported at 1700 cm^{-1} [22]. Nataraj et al. [24] reported υC=O vibrations of the aldehyde group at 1674 cm^{-1} (IR) and at 1672 cm^{-1} (Raman) for 2-hydroxy-5-bromobenzaldehyde. For the title compound these vibrations are assigned at 1729, 1728 cm^{-1} theoretically (B3LYP). In the present case, the γCH vibrations of the aldehyde groups are assigned at 995, 994 cm^{-1} (B3LYP).

In the present discussion, the phenyl rings attached to the anthraquinone core at C_{12} and C_{16} are designated as PhII and PhIII, respectively. The anthraquinone core system is designated as PhI. The phenyl CH stretching modes occurs above 3000 cm^{-1} and is typically exhibited as multiplicity of weak to moderate bands compared with the aliphatic CH stretching [25]. In the present case, the B3LYP calculations give υCH modes of the phenyl rings PhII and PhIII in the range 3096–3056 cm^{-1}. Experimentally these bands are observed at 3068 cm^{-1} (IR) and 3070 cm^{-1} (Raman).

For para-substituted benzenes, the δCH modes are seen in the range 970–1315 cm^{-1} [26]. In the present case in-plane CH deformation bands are assigned at 1280, 1151, 1096, 976 cm^{-1} for PhII and at 1280, 1154, 1096, 993 cm^{-1} for PhIII theoretically (B3LYP). Experimentally these bands are observed at 1092 cm^{-1} (IR), 1092 cm^{-1} (Raman) for both PhII and PhIII. The CH out-of-plane deformations are observed in the range 1000–700 cm^{-1} [26]. Generally, the CH out-of-plane deformations with the highest wavenumbers are weaker than those absorbing at lower wavenumbers. In the present case these γCH modes are observed at 834 cm^{-1} (IR) for PhIII and 919 cm^{-1} (Raman), 920, 828 cm^{-1} (IR) for PhII. Theoretically these modes are assigned at 926, 896, 831, 812 cm^{-1} (B3LYP) for PhIII and at 944, 925, 829, 798 cm^{-1} (B3LYP) for PhII. The strong CH out-of-plane deformation band occurring at 840 ± 50 cm^{-1} is typical for 1,4-di-substituted benzenes [26]. For the title compound, a band is observed at 828 for PhII and at 834 cm^{-1} for PhIII in the IR spectrum and is assigned as γCH modes.

The benzene ring possesses six ring-stretching vibrations of which the four with the highest wavenumbers occurring near 1600, 1580, 1490 and 1440 cm^{-1} are good group vibrations [26]. With heavy substituents, the bands tend to shift to somewhat lower wavenumbers, and the greater the number of substituents on the ring, the broader the absorption regions [26]. In the case of C=O substitution, the band near 1490 cm^{-1} can be very weak [26]. The fifth ring-stretching vibration is active near 1315 ± 65 cm^{-1}, a region that overlaps strongly with that of the CH in-plane deformation [26]. The sixth ring-stretching vibration, the ring breathing mode, appears as a weak band near 1000 cm^{-1}

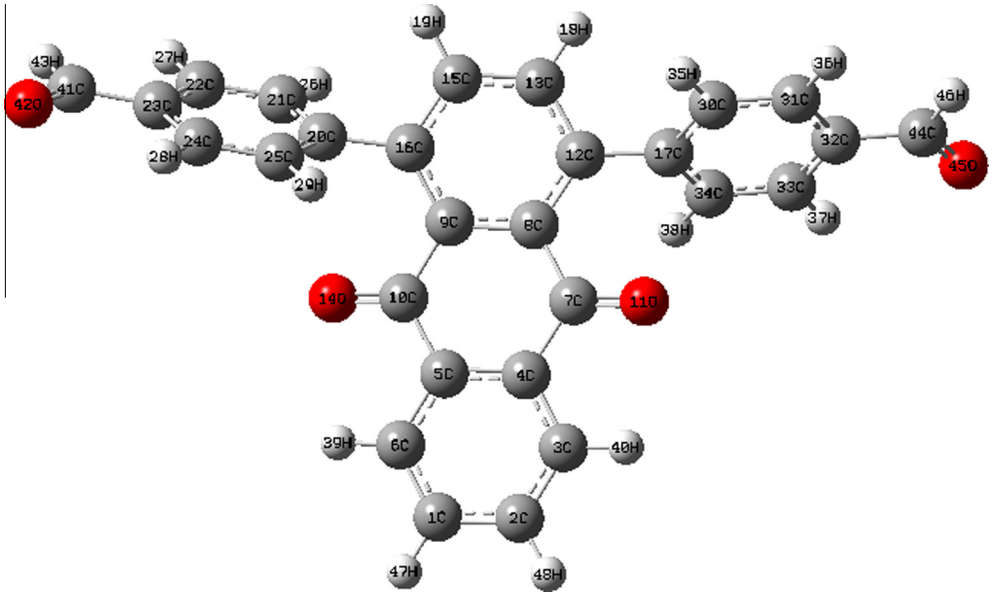

Fig. 3. Optimized Geometry of 1,4-bis(4-formylphenyl)anthraquinone (B3LYP/6-31G*).

in mono-, 1,3-di-, and 1,3,5-trisubstituted benzenes. In the otherwise substituted benzenes, however, this vibration is substituent sensitive [26]. For the title compound these bands are observed at 1603, 1537, 1415 cm^{-1} (IR), 1607 cm^{-1} (Raman) for PhII and at 1484 cm^{-1} (IR) for PhIII experimentally. In the present case the phenyl ring stretching vibrations are assigned at 1600, 1556, 1494, 1406, 1295 cm^{-1} for PhII and at 1598, 1568, 1491, 1403, 1294 cm^{-1} for PhIII, theoretically. Some phenyl ring stretching modes υPh are not pure, but contain significant contributions from other modes also. The ring-breathing modes for the para-substituted benzenes with entirely different substituents were reported to be strongly IR active with typical bands in the interval 780–840 cm^{-1} [27]. These vibrations are assigned at 774 cm^{-1} for PhII and at 785 cm^{-1} for PhIII theoretically (B3LYP). A medium intense band observed at 756 cm^{-1} in the IR spectrum is assigned as ring breathing mode of PhII. The ring-breathing mode of para-substituted benzenes were reported at 804 and 792 cm^{-1} experimentally and at 782 and 795 cm^{-1} theoretically [28,29].

The ring PhI stretching modes are assigned in the range 997–1583 cm^{-1} theoretically (B3LYP) and corresponding bands are observed at 1570, 1515, 1454, 1319, 1287, 1070, 1014 cm^{-1} in the IR spectrum and at 1539, 1454, 1318 cm^{-1} in the Raman spectrum. Most of the modes are not pure but contains significant contributions from other modes also. Jorge-Villar and Edwards [30] reported the characteristic bands of anthraquinone pigment, atranorin at 1666, 1658, 1588, 1438, 1377, 1304, 1294, 1265, 1111, 902, 861, 824, 781, 584, 467, 422, 384 cm^{-1} in the Raman spectrum. Baran et al. [31] reported the PhI stretching modes at 1273, 1143, 1090, 1044, 1027 cm^{-1} and bending modes at 1292, 823 cm^{-1}. Leeo and Boo [32] reported the anthracene ring stretching modes at 1156, 1245, 1298, 1335, 1388, 1402, 1406, 1493, 1534, 1584, 1615 cm^{-1} experimentally and at 1149, 1261, 1300, 1369, 1378, 1399, 1501, 1526, 1537, 1588, 1596 cm^{-1} theoretically. Anthracene ring stretching modes were reported at 1434, 1454, 1459, 1564 cm^{-1} by Zilberg et al. [33], 1616, 1450 cm^{-1} by Kafer et al. [34], 1242, 1265, 1398, 1527, 1547, 1607 cm^{-1} (experimental), 1252, 1265, 1391, 1536, 1560, 1627 cm^{-1} (calculated) by Wang et al. [35]. The anthracene vibrational modes were reported at 1258, 1395, 1560 cm^{-1} [36] and for 9-phenylanthracene these modes were reported at 1264, 1391, 1567 cm^{-1} [37].

For the title compound the in-plane CH deformation modes of the anthraquinone ring are assigned at 1262, 1218, 1163, 1146, 1053, 1022 (B3LYP), 1264, 1169, 1035 cm^{-1} in the Raman spectrum and at 1260, 1169, 1035 cm^{-1} in the IR spectrum. The CH deformation bands of anthracene ring were reported at 560, 613, 644, 659, 722, 761, 784, 816, 822, 842, 879, 886, 943, 1156, 1233, 1258 cm^{-1} (experimental), 550, 601, 627, 642, 702, 745, 764, 798, 813, 827, 835, 868, 870, 925, 1020, 1022, 1149, 1219, 1238 cm^{-1} (DFT) [32]. Kafer et al. [34] reported the CH deformations bands of the anthracene ring at 1300, 1073, 954, 893, 735 cm^{-1} and Zilberg et al. [33] reported these bands at 719, 779, 886 cm^{-1}. Wang et al. [35] reported the CH deformation bands at 715, 1026, 1036, 1130 cm^{-1} experimentally and at 708, 1029, 1030, 1136 cm^{-1} theoretically. In the present case the out-of-plane CH modes of the anthraquinone ring are assigned in the range 797–957 cm^{-1} theoretically (B3LYP). Experimentally these bands are observed at 958, 793 cm^{-1} in the IR spectrum and at 961, 848 cm^{-1} in the Raman spectrum. For the title compound the in-plane and out-of-plane anthraquinone ring deformations are observed below 800 cm^{-1} (Table 1) and are in agreement with reported values [32,34,35]. Chandran et al. [38] reported the anthracene ring modes in the range 1267–1625 (IR), 1255–1625 cm^{-1} (Raman), 1259–1622 cm^{-1} (DFT), CH in-plane deformations at 1097, 1170, 1253 cm^{-1} (IR), 1017, 1228 cm^{-1} (Raman), in the range 1022–1291 cm^{-1} (DFT) and out-of-plane CH modes at 955 (IR), 971, 857 (Raman) and in the range 990–846 cm^{-1} theoretically. Anthracene ring deformations were reported at 369, 502, 575, 592, 602, 703, 709 cm^{-1} (experimental), 353, 493, 573, 594, 607, 693 cm^{-1} (DFT) [32].

Infrared active C=O stretching vibrations for anthraquinones were reported in the region 1680–1630 cm^{-1}, with anthraquinone itself at 1676 cm^{-1} [39], 2-methylanthraquinone at 1672 cm^{-1} [14], 1,4-dimethylanthraquinone at 1668 cm^{-1} [14]. Baran et al. [31] published the Raman spectrum of the 1,2-dihydroxyanthraquinone, alizarin, adsorbed on a silver surface with υC=O at 1657 and at 1629 cm^{-1}, where it is known that the intramolecular hydrogen bonding from the hydroxyl group to the quinone carbonyl function decreases the band frequency versus a non-complexed carbonyl function. Krishnakumar and Xavier [40] reported the Raman spectrum of 1,5-dichloroanthraquinone. Joseph et al. [11] reported C=O stretching vibrations at 1669, 1600 cm^{-1} in the IR spectrum

Table 1
IR, Raman bands and calculated (scaled) wavenumbers of 1,4 bis(4-formylphenyl)anthraquinone and assignments.

B3PW91/6-31G*			B3LYP/6-31G*			IR	Raman	Assignments[a]
υ	IR_I	R_A	υ	IR_I	R_A	υ	υ	
3114	12.09	202.64	3107	10.78	183.59	–	–	υCHI(100)
3112	0.40	29.98	3105	0.70	27.40	–	–	υCHI(94)
3104	0.88	199.43	3096	0.97	195.22	–	–	υCHII(95)
3104	5.26	22.12	3096	5.49	22.56	–	–	υCHIII(95)
3098	7.34	163.11	3090	9.24	163.07	–	–	υCHI(98)
3096	14.56	213.32	3086	19.08	236.18	–	–	υCHI(100)
3089	14.77	40.79	3079	16.43	41.59	–	–	υCHIII(51), υCHII(47)
3089	1.73	130.88	3079	1.93	133.61	–	–	υCHII(51), υCHIII(47)
3084	10.29	15.69	3075	11.32	41.15	–	–	υCHI(98)
3084	2.31	58.92	3074	2.87	59.28	–	–	υCHII(97)
3083	6.16	58.43	3074	9.68	36.79	–	–	υCHIII(97)
3082	2.90	79.21	3072	3.46	82.19	3068	3070	υCHI(95)
3066	4.38	132.73	3057	4.73	132.59	–	–	υCHII(50), υCHIII(49)
3066	20.24	57.31	3056	22.55	56.86	–	–	υCHIII(50), υCHII(49)
2803	66.18	310.07	2794	64.96	300.57	–	–	υC41H43(58), υC44H46(41)
2803	296.39	103.68	2793	297.55	99.80	2725	–	υC41H43(41), υC44H46(58)
1744	0.65	502.45	1729	0.74	468.96	–	–	υC44=O45(42), υC41=O42(40)
1743	636.84	11.37	1728	621.43	10.73	–	–	υC44=O45(40), υC41=O42(42)
1704	376.11	3.37	1686	366.09	2.60	1692	1690	υC7=O11(38), υC10=O14(38)
1698	4.08	359.68	1679	4.01	361.16	1678	1671	υC10=O14(38), υC7=O11(38)
1611	7.93	1859.58	7.82	1790.89	1603	1	–	υPhIII(26), υPhII(55)
1609	253.50	169.96	1598	254.34	165.03	–	–	υPhIII(56), υPhII(26)
1595	59.44	119.10	1583	63.83	122.34	1570	–	υPhI(54), υPhII(17), δCHI(12)
1590	1.02	194.76	1578	0.77	207.50	–	–	υPhI(76)
1580	0.06	350.63	1568	0.13	363.24	–	–	υPhIII(72)
1568	62.54	3.05	1556	65.94	3.11	1537	–	υPhIII(34), υPhII(59)
1567	2.51	36.92	1554	2.57	41.46	–	1539	υPhI(56), υPhII(25)
1534	11.16	37.02	1523	13.01	42.57	1515	–	υPhI(72), δCHI(12)
1498	7.31	16.11	1494	5.38	10.10	–	–	υPHIII(16), υPhII(66)
1494	0.82	43.25	1491	0.61	35.40	1484	–	δCHII(15), υPhIII(64)
1467	4.53	8.07	1467	2.07	7.82	1454	1454	δCHI(16), υPhI(58)
1448	4.40	8.68	1442	3.12	2.20	–	–	υPhI(66), δCHI(18)
1441	0.32	12.87	1437	0.92	17.78	–	–	δCHI(36), υPhI(59)
1407	8.00	28.27	1406	4.40	30.43	1415	–	υPhII(21), υPhII(66)
1404	12.11	0.30	14.03	7.50	0.21	–	–	υPhII(13), υPhIII(63)
1380	7.32	9.18	1380	10.07	10.38	–	–	δC44H46(30), δC41H43(28), υPhII(11)
1379	30.54	1.86	1379	37.45	1.96	1381	–	δC44H46(31), δC41H43(30), υPhIII(5)
1367	33.42	13.32	1356	19.16	14.34	–	–	υPhI(59), δCHI(12)
1349	0.71	3.89	1328	0.33	5.45	–	–	υPhI(72), υPhII(15)
1320	107.0	173.94	1301	144.15	222.82	1319	1318	υPhI(63)
1313	45.84	0.08	1295	55.70	0.08	–	–	υPhII(66), υPhIII(16)
1310	55.97	53.35	1294	9.35	21.14	–	–	υPhII(63), υPhII(23)
1288	0.76	79.82	1284	3.04	32.01	1287	–	υPhI(60), υCC(22)
1280	16.38	0.06	1280	0.53	46.36	–	–	δCHIII(59), δCHII(35)
1280	64.09	5.45	1280	98.07	17.01	–	–	δCHII(52), δCHIII(38)
1264	0.24	5.00	1262	1.22	7.41	1260	1264	δCHI(51), υCC(46)
1261	63.03	382.04	1245	11.30	446.66	–	–	υPhI(49), υCC(44)
1250	364.06	288.15	1238	397.62	167.94	1248	–	υPhI(18), υCC(61)
1218	3.83	3.57	1218	4.52	5.14	–	–	δCHI(60), υPhI(27)
1199	12.23	81.92	1194	12.81	85.42	1211	1211	υCC(35), δPhIII(13)
1198	172.19	2.53	1194	150.08	2.38	1211	1211	υCC(35), δPhII(13)
1164	1.91	61.78	1163	0.67	59.78	1169	1169	δCHI(50), υPhI(10)
1154	0.91	161.40	1155	1.89	193.80	–	–	υPhI(75), δCHII(12)
1154	68.51	10.99	1154	86.81	13.27	–	–	δCHIII(41), δCHII(28)
1153	16.74	0.14	1151	13.68	0.12	–	–	δCHII(44), δCHIII(28)
1145	12.08	17.02	1146	13.18	19.18	–	–	δCHI(89)
1096	8.40	4.06	1096	6.02	3.41	1092	1092	δCHIII(65), δCHII(24)
1095	10.65	0.13	1096	8.77	3.12	1092	1092	δCHII(61), δCHIII(26)
1080	20.94	33.75	1077	0.34	1.84	–	–	υPhI(56), δCHI(10)
1077	0.12	1.56	1075	29.12	36.65	1070	–	υPhI(49), δCHI(23)
1056	17.56	3.59	1053	22.72	3.68	–	–	υPhI(10), υPhII(12), δCHI(49)
1025	2.21	47.91	1022	1.57	52.38	1035	1035	υPhI(29), δCHI(46), υPhII(13)
997	6.22	14.89	997	5.03	14.21	1014	–	υPhI(78), δCHI(11)
995	9.25	1.65	995	13.76	0.39	–	–	γC41H43(52), γCHIII(10)
994	0.96	9.08	994	0.50	9.23	–	–	γC44H46(56), τPhI(14)
994	3.76	9.39	993	1.05	11.09	981	–	δCHII(23), δCHIII(63)
978	0.43	0.18	976	0.39	0.22	–	–	δCHII(48), δPhI(32)
958	1.18	0.35	957	1.04	0.40	958	961	γCHI(90)
952	16.85	10.35	951	1.81	2.81	–	–	γCHI(55), δPhI(32)
951	0.19	0.21	950	0.14	0.26	–	–	δPhI(48), γCHI(25)
951	8.99	4.47	949	7.70	8.84	–	–	γCHI(78)
947	34.50	5.70	944	53.16	9.04	–	–	CHII(55), δC7=O11(28), δC10=O14(22)
928	0.08	2.79	926	0.01	2.87	–	–	γCHIII(60), γCHII(31)

(*continued on next page*)

Table 1 (*continued*)

B3PW91/6-31G*			B3LYP/6-31G*			IR	Raman	Assignments[a]
υ	IR_I	R_A	υ	IR_I	R_A	υ	υ	
927	0.49	4.22	925	0.47	4.51	920	919	γCHII(59), γCHIII(27)
896	5.92	11.36	896	6.56	12.27	–	–	γCHIII(72), τPhI(13)
887	0.03	4.18	887	0.02	4.46	–	–	γCHI(75)δPhI(19), δC═O(18)
844	2.91	5.46	845	2.51	5.43	–	848	γCHI(64)
833	45.74	5.84	831	30.48	5.87	–	–	γCHIII(52), γCHI(16)
831	2.99	40.79	829	18.32	9.03	828	–	τPhI(13), γC═O(18), γCHII(60)
828	3.83	41.23	828	0.02	6.15	–	–	γCHIII(32), γCHII(51)
828	9.89	5.70	827	6.59	76.24	–	–	τPhI(47), γCHII(19), γCHIII(19)
812	64.66	2.01	812	59.57	2.38	–	–	δPhII(14), δPhIII(14), υCC(12)
810	41.49	3.97	812	37.30	5.18	–	–	γCHIII(56), γCHII(26)
799	5.78	18.89	798	2.90	16.94	–	–	γCHII(54), γCHIII(34)
797	58.02	0.63	797	62.07	0.81	793	–	γCHI(56), γC═O(26)
785	10.78	1.09	785	9.64	1.34	–	–	υPhII(68), δPhI(10)
775	45.31	3.52	774	45.54	3.44	756	–	δPhI(20), υPhII(54)
730	0.90	0.78	730	0.76	0.82	731	–	τPhI(65), γCC(18)
721	14.90	1.53	722	9.76	1.78	–	–	τPhII(14), τPhIII(14)γCHI(18), γC═O(12)
717	35.39	3.75	717	33.70	3.74	–	–	τPhII(23), τPhIII(23)
710	0.09	7.97	710	0.05	7.84	–	–	τPhIII(35), τPhII(34), γCC(12)
702	21.48	0.25	702	22.16	0.19	–	–	δPhI(22), δC═O(16), τPhII(12)
668	18.71	0.65	670	19.46	0.64	684	–	δPhI(23), δPhIII913), δC═O(14)
661	0.73	1.28	662	0.80	1.56	664	665	τPhI(56), γC═O(13)
648	2.45	26.17	648	2.66	26.01	644	–	δPhI(21), δPhII(18)
630	4.19	1.94	632	3.89	2.19	–	–	δPhIII(19), δPhII(19), δPhI(16)
627	7.61	5.72	629	7.80	6.00	625	630	δPhI(53), δPhII(17)
616	1.89	1.72	618	0.14	8.52	–	–	δPhI(47), δPhII(19)
615	0.11	8.35	617	1.41	1.55	601	–	δPhIII(37), δPhII(35)
586	10.60	0.08	588	9.88	0.07	–	–	τPhI(20), γCC(30), δPhII(12), δPhIII(12)
542	3.08	2.80	543	2.45	3.08	542	–	τPhII(11), τPhIII(11), γCC(28), δCC(14)
530	13.24	20.84	533	10.67	20.25	522	–	τPhIII(14), τPhII(14), γCC(38)
510	5.09	4.07	510	4.73	3.54	504	–	δPhI(36), τPhII(22)
491	0.71	9.11	493	0.47	9.47	–	486	τPhI(67), τPhII(15)
470	0.51	11.16	471	0.49	11.02	473	472	τPhI(35), τPhII(23)
457	2.09	27.30	458	1.95	28.65	450	–	δPhIII(32), δPhII(14), δCC(12)
425	1.58	0.28	427	1.57	0.41	–	–	τPhI(53), γC═O(12)
425	0.03	3.86	426	0.04	3.77	–	–	δPhI(30), τPhI(17)
411	0.01	0.22	414	0.05	0.21	419	416	τPhI(68), τPhII(10)
405	0.15	30.08	408	0.18	29.69	–	–	τPhIII(34), τPhII(34)
404	0.67	3.90	406	0.55	3.90	–	–	τPhII(34), τPhII(34)
403	8.33	15.86	405	8.26	15.91	–	–	τPhI(44), γCHI(12)
385	2.73	0.41	387	2.39	0.43	–	–	τPhII(21), δC═O(20)
382	10.28	5.30	383	11.64	5.52	–	–	τPhIII(25), γCC(16)
367	22.26	5.59	368	20.64	5.18	–	–	δPhI(25), δC═O(14), γCC(12)
305	1.57	4.39	308	2.09	5.74	–	313	γCC(24), δPhI(10)
304	3.59	4.89	304	2.97	4.51	–	–	δPhI(27), δC═O(24)
295	10.54	12.05	299	10.29	10.14	–	272	δPhI(23), τPhI(21)
253	1.46	3.34	255	1.38	3.31	–	–	τC═O(12), γCC(20)
228	0.84	0.62	229	1.01	0.74	–	–	δPhI(40), δPhII(14)
217	4.06	2.76	221	3.79	2.75	–	226	δCC(50), δC═O(12)
212	7.93	4.97	215	7.61	4.97	–	–	τPhI(50), δCC(22)
192	2.67	3.34	193	2.68	3.37	–	188	τC═O(38), τPhI(13), τPhII(13)
169	2.62	5.42	170	2.61	5.30	–	–	τC═O(46), τPhII(14)
164	8.82	2.44	166	8.24	2.54	–	–	τPhI(40), δCC(22)
163	0.45	4.21	164	0.43	4.12	–	–	δPhI(46), δCC(20)
142	1.30	0.42	143	1.59	0.44	–	–	τPhI(61), γC═O(16)
122	2.51	5.72	122	2.56	5.74	–	–	τPhI(50), τC═O(16)
115	4.98	1.98	116	4.85	2.00	–	–	τPhI(29), τC═O(16)
113	2.67	0.23	114	2.52	0.22	–	–	τC═O(28), γCC(28)
98	0.01	3.43	99	0.02	3.38	–	104	τPhI(40), γCC(36)
56	0.86	1.99	56	0.86	1.91	–	–	τPhI(32), τCC(27)
49	0.83	18.74	49	0.84	18.61	–	–	τCC(24), γCC(20), τPhI(16)
40	0.14	9.87	40	0.08	10.26	–	–	τCO(29), τCC(23)
31	0.10	6.67	31	0.16	6.53	–	–	γCC(22), τCC(22), τPhII(14)
24	3.37	4.61	24	3.28	4.02	–	–	τPhI(53), τPhII(13)
21	1.02	5.65	21	1.14	6.52	–	–	τPhI(40), τCC(35), γCC(12)
20	1.61	5.50	19	1.60	6.28	–	–	τC—C(45), τPhI(41)

[a] υ-stretching; δ-in-plane deformation; γ-out-of-plane deformation; τ-torsion; as-asymmetric; s-symmetric; The phenyl rings attached to the anthraquinone core at C_{12} and C_{16} are designated as PhII and PhIII, respectively. The anthraquinone core system is designated as PhI; IRI-IR intensity; RA-Raman activity; potential energy distribution are given in brackets in the assignment column.

for 1-(4-methoxyphenyl)-4-methylanthraquinone. For the title compound, the bands at 1686 and 1679 cm^{-1} (B3LYP) are assigned as C═O stretching modes. Experimentally these vibrations are observed at 1692, 1678 cm^{-1} (IR) and 1690, 1671 cm^{-1} (Raman). The in-plane δC═O and out-of-plane γC═O deformation bands were also identified and assigned (Table 1).

Geometrical parameters

To best of our knowledge, the XRD of the title compound is not yet reported. In the present discussion the geometrical parameters of the title compound given by B3LYP calculations are compared with the geometrical parameters of similar derivatives. From the X-ray crystal structures of substituted anthraquinones, it is evident that the C=O bond length depends on the substitution pattern. For anthraquinone derivatives, C=O bond lengths were reported in the range 1.2103–1.2233 Å [41–43]. The author's calculation of 1.2246 Å (B3LYP) for the C=O bond lengths (C_7=O_{11} and C_{10}—O_{14}) of the title compound are in agreement with the reported values. Boonnak et al. [44] reported the C_7=O_{11} and C_{10}=O_{14} bond lengths as 1.2604 Å and 1.2234 Å respectively. Further calculated bond length values of the title compound, C_4—C_5 = 1.4027 Å, C_9—C_8 = 1.4199 Å, C_7—C_8 = 1.5028 Å, C_9—C_{10} = 1.5028 Å, C_4—C_7 = 1.4876 Å, C_5—C_{10} = 1.4876 Å, are comparable to the values, 1.428, 1.408, 1.480, 1.488, 1.464, 1.451 Å reported for purpurin (1,2,4-trihydroxyanthraquinone) [45].

For the title compound, the C—C bond lengths for the phenyl rings PhII and PhIII lie between 1.3859 Å to 1.4075 Å. Here for the title compound, benzene rings are a regular hexagon with bond lengths somewhere in between the normal values for a single (1.54 Å) and a double bond (1.33 Å) [46]. According to our calculations, at C_7 position, the exocyclic angle C_8—C_7—O_{11} is increased by 1.1° from 120°, which shows the interaction between H_{40} and O_{11}. At C_{10} (C_5—C_{10}—O_{14} = 120.2°, C_9—C_{10}—O_{14} = 121.3°), there is also an interaction between H_{39} and O_{14}. This departure of the exocyclic angles from 120° can be found in the crystal structures of the anthraquinones, also [47].

The anthraquinone core is not planar as is evident from the calculated torsion angles, C_2—C_3—C_4—C_7 = −179.7°, C_3—C_4—C_7—O_{11} = −5.7°, C_6—C_5—C_4—C_7 = 179.6°, C_5—C_4—C_7—O_{11} = 174.2°, C_1—C_6—C_5—C_{10} = −179.7°, C_6—C_5—C_{10}—O_{14} = −5.7°, C_3—C_4—C_5—C_{10} = 179.6°, C_4—C_5—C_{10}—O_{14} = 174.2°, C_{13}—C_{12}—C_8—C_7 = −171.3°, C_{12}—C_8—C_7—C_4 = −173.3°, C_{15}—C_{16}—C_9—C_{10} = −171.3° and C_{16}—C_9—C_{10}—C_5 = −173.3°. The X-ray crystal structure of anthraquinones, especially of hindered arylanthraquinones, shows a significant distortion of the anthraquinone core [48].

The C—C bond length in the anthracene ring is in the range 1.3895–1.5028 Å, whose values are similar to those of the other substituted anthracenes [49]. Fan and Chen [50] and Suwunwong et al. [51] reported the anthracene C—C bond lengths in the range 1.3572–1.4407 Å and 1.3563–1.4402 Å respectively. Silva et al. [52] reported the bond lengths and bond angles of anthracene ring as C_7—C_8 = 1.4088, C_7—C_4 = 1.4308, C_5—C_4 = 1.4180, C_5—C_{10} = 1.3928, C_{10}—C_9 = 1.3978, C_9—C_8 = 1.4378 Å and C_4—C_7—C_8 = 120.4°, C_7—C_4—C_5 = 119.7°, C_7—C_8—C_9 = 119.2°, C_{10}—C_5—C_4 = 119.2°, C_5—C_{10}—C_9 = 122.4°, C_{10}—C_9—C_8 = 119.2° whereas in the present case the corresponding values are 1.5028, 1.4876,1.4027, 1.4876, 1.5028, 1.4199 Å and 118.5, 121.0, 119.7, 121.0, 118.5, 119.7°. For the title compound, the calculated values of the C—H and C=O bond lengths in the aldehyde groups are 1.1132 Å and 1.2166 Å respectively, whereas the reported values are 1.11 Å and 1.20 Å respectively [23].

First hyperpolarizability

Nonlinear optics deals with the interaction of applied electromagnetic fields in various materials to generate new electromagnetic fields, altered in wavenumber, phase, or other physical properties [9]. Organic molecules able to manipulate photonic signals efficiently are of importance in technologies such as optical communication, optical computing, and dynamic image processing [10,53]. In this context, the dynamic first hyperpolarizability of the title compound is also calculated in the present study. The first hyperpolarizability (β_0) of this novel molecular system is calculated using DFT method, based on the finite field approach. In the presence of an applied electric field, the energy of a system is a function of the electric field. First hyperpolarizability is a third rank tensor that can be described by a $3 \times 3 \times 3$ matrix. The 27 components of the 3D matrix can be reduced to 10 components due to the Kleinman symmetry [54]. The components of β are defined as the coefficients in the Taylor series expansion of the energy in the external electric field. When the electric field is weak and homogeneous, this expansion becomes

$$E = E_0 - \sum_i \mu_i F^i - \frac{1}{2}\sum_{ij} \alpha_{ij} F^i F^j - \frac{1}{6}\sum_{ijk} \beta_{ijk} F^i F^j F^k - \frac{1}{24}\sum_{ijkl} \gamma_{ijkl} F^i F^j F^k F^l + \ldots$$

where E_0 is the energy of the unperturbed molecule, F_i is the field at the origin, μ_{ij}, α_{ij}, β_{ijk} and γ_{ijkl} are the components of dipole moment, polarizability, the first hyperpolarizabilities, and second hyperpolarizabilities, respectively. The calculated first hyperpolarizability of the title compound is 8.04×10^{-30} esu, which is comparable with the reported values of similar derivatives [11,55]. The calculated hyperpolarizability of the title compound is 61.85 times that of the standard NLO material urea (0.13×10^{-30} esu) [56]. We conclude that the title compound is an attractive object for future studies of nonlinear optical properties.

NBO analysis

The natural bond orbitals (NBO) calculations were performed using NBO 3.1 program [57] as implemented in the Gaussian09 package at the B3LYP/6-31G* level in order to understand various second-order interactions between the filled orbitals of one subsystem and vacant orbitals of another subsystem, which is a measure of the intermolecular delocalization or hyper conjugation. NBO analysis provides the most accurate possible 'natural Lewis structure' picture of 'j' because all orbital details are mathematically chosen to include the highest possible percentage of the electron density. A useful aspect of the NBO method is that it gives information about interactions of both filled and virtual orbital spaces that could enhance the analysis of intra and inter molecular interactions.

The second-order Fock-matrix was carried out to evaluate the donor–acceptor interactions in the NBO basis. The interactions result in a loss of occupancy from the localized NBO of the idealized Lewis structure into an empty non-Lewis orbital. For each donor (i) and acceptor (j) the stabilization energy (E2) associated with the delocalization i → j is determined as

$$E(2) = \Delta E_{ij} = q_i \frac{(F_{i,j})^2}{(E_j - E_i)}$$

q_i → donor orbital occupancy, E_i, E_j → diagonal elements, F_{ij} → the off diagonal NBO Fock matrix element.

In NBO analysis large $E(2)$ value shows the intensive interaction between electron donors and electron-acceptors, and greater the extent of conjugation of the whole system, the possible intensive interaction are given in Table S2 as supplementary material. The second order perturbation theory analysis of Fock-matrix in NBO basis shows strong intermolecular hyper conjugative interactions are formed by orbital overlap between n(O) and σ*(C—C) bond orbitals which result in ICT causing stabilization of the system. These interactions are observed as an increase in electron density (ED) in C—C anti bonding orbital that weakens the respective bonds. There occurs a strong inter molecular hyper conjugative interaction of C_7—C_8 from O_{11} of $n_2(O_{11})$ → σ*(C_7—C_8)

which increases ED (0.06481 e) that weakens the respective bonds C_7—C_8 (1.5028 Å) leading to stabilization of 20.16 kJ/mol and also the hyper conjugative interaction of C_9—C_{10} from O_{14} of $n_2(O_{14}) \rightarrow \sigma^*(C_9—C_{10})$ which increases ED (0.06481 e) that weakens the respective bonds C_9—C_{10} (1.5028 Å) leading to stabilization of 20.16 kJ/mol. Also the hyperconjugative interaction of C_{23}—C_{41} from O_{42} of $n_2(O_{42}) \rightarrow \sigma^*(C_{23}—C_{41})$ which increases ED (0.05998 e) that weakens the respective bonds C_{23}—C_{41} (1.4784 Å) leading to stabilization of 18.93 kJ/mol. An another hyperconjugative interaction observed in C_{32}—C_{44} from O_{45} of $n_2(O_{45}) \rightarrow \sigma^*(C_{32}—C_{44})$ which increases ED (0.05998 e) that weakens the respective bond C_{32}—C_{44} (1.4784 Å) leading to a stabilization of 18.93 kJ/mol.

The increased electron density at the carbon atoms leads to the elongation of respective bond length and a lowering of the corresponding stretching wave number. The electron density (ED) is transferred from the n(O) to the anti-bonding π^* orbital of the C—C explaining both the elongation and the red shift [58]. The hyper conjugative interaction energy was deduced from the second-order perturbation approach. Delocalization of electron density between occupied Lewis-type (bond or lone pair) NBO orbitals and formally unoccupied (anti bond or Rydberg) non-Lewis NBO orbitals corresponds to a stabilizing donor–acceptor interaction. The —C=O stretching modes can be used as a good probe for evaluating the bonding configuration around the corresponding atoms and the electronic distribution of the molecule. Hence the title compound is stabilized by these orbital interactions.

The NBO analysis also describes the bonding in terms of the natural hybrid orbital $n_2(O_{11})$, which occupy a higher energy orbital (−0.27178 a.u.) with considerable p-character (100.0%) and low occupation number (1.88002) and the other $n_1(O_{11})$, which occupy a lower energy orbital (−0.69845 a.u.) with considerable p-character (42.21%) and high occupation number (1.97814). Also $n_2(O_{14})$, which occupy a higher energy orbital (−0.27178 a.u.) with considerable p-character (100.0%) and low occupation number (1.88002) and the other $n_1(O_{14})$, which occupy a lower energy orbital (−0.69845 a.u.) with considerable p-character (42.21%) and high occupation number (1.97814). Again $n_2(O_{42})$, which occupy a higher energy orbital (−0.25941 a.u.) with considerable p-character (99.76%) and low occupation number (1.88299) and the other $n_1(O_{42})$, which occupy a lower energy orbital (−0.68887 a.u.) with considerable p-character (41.65%) and high occupation number (1.98348). Also $n_2(O_{45})$, which occupy a higher energy orbital (−0.25941 a.u.) with considerable p-character (99.76%) and low occupation number (1.88299) and the other $n_1(O_{45})$, which occupy a lower energy orbital (−0.68887 a.u.) with considerable p-character (41.60%) and high occupation number (1.98348). Thus, a very close to pure p-type lone pair orbital participates in the electron donation to the σ^*(C—C) orbitals for n(O) → σ^*(C—C) interactions in the compound. The result is tabulated in Table S3 as supporting material.

Mulliken charges

Mulliken charges are calculated by determining the electron population of each atom as defined in the basis functions. The charge distributions calculated by the Mulliken [59,60] and NBO methods for the equilibrium geometry of 1,4-bis(4-formylphenyl)anthraquinone are given in Table S4 as supporting information. The charge distribution on the molecule has an important influence on the vibrational spectra. In 1,4-bis(4-formylphenyl)anthraquinone, the Mulliken atomic charge of the carbon atoms in the neighbourhood of C_7 and C_{10} become more positive, shows the direction of delocalization and shows that the natural atomic charges are more sensitive to the changes in the molecular structure than Mulliken's net charges. The results are given in Fig. S1 as supporting material. Also we done a comparison of Mulliken charges obtained by different basis sets and tabulated (Table S5 supporting material) in order to assess the sensitivity of the calculated charges to changes in (i) the choice of the basis set; (ii) the choice of the quantum mechanical method. The results can, however, better be represented in graphical form (Fig. S2 supporting material). We have observed a change in the charge distribution by changing different basis sets.

PES scan studies

A detailed potential energy surface (PES) scan on dihedral angles C_{21}—C_{20}—C_{16}—C_{15} and C_{30}—C_{17}—C_{12}—C_8 have been performed at B3LYP/6-31G(d) level to reveal all possible conformations of 1,4-bis(4-formylphenyl)anthraquinone. The PES scan was carried out by minimizing the potential energy in all geometrical parameters by changing the torsion angle at every 20° for a 180° rotation around the bond. The results obtained in PES scan study are plotted in Figs. 4 and 5. For the C_{21}—C_{20}—C_{16}—C_{15} rotation, the minimum energy was obtained at 59.6° in the potential energy curve of energy −1377.50988 Hartrees. For the C_{30}—C_{17}—C_{12}—C_8 rotation, the minimum energy occurs at −124.0° in the potential energy curve of energy −1377.50981 Hartrees.

Molecular electrostatic potential

MEP is related to the ED and is a very useful descriptor in understanding sites for electrophilic and nucleophilic reactions as well as hydrogen bonding interactions [61,62]. The electrostatic potential $V(r)$ is also well suited for analyzing processes based on the "recognition" of one molecule by another, as in drug-receptor, and enzyme-substrate interactions, because it is through their potentials that the two species first "see" each other [63,64]. To predict reactive sites of electrophilic and nucleophilic attacks for the investigated molecule, MEP at the B3LYP/6-31G(d,p) optimized geometry was calculated. The negative (red and yellow) regions of MEP were related to electrophilic reactivity and the positive (blue) regions to nucleophilic reactivity (Fig. 6). From the MEP it is evident that the negative charge covers the C=O in the anthraquinone and aldehyde groups and the positive region is over the C—C bonds of the rings.

HOMO–LUMO band gap

HOMO and LUMO are the very important parameters for quantum chemistry. The conjugated molecules are characterized by a highest occupied molecular orbital-lowest unoccupied molecular orbital (HOMO–LUMO) separation, which is the result

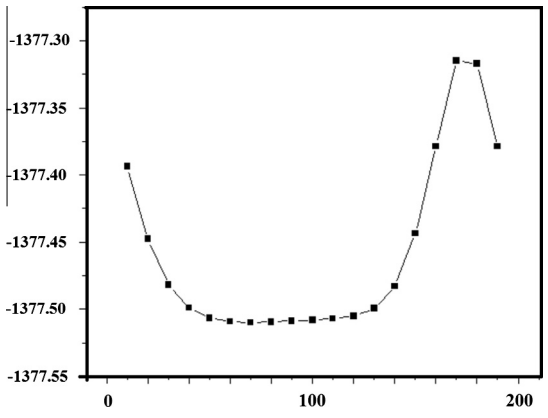

Fig. 4. Profile of potential energy scan for the torsion angle C_{21}—C_{20}—C_{16}—C_{15}.

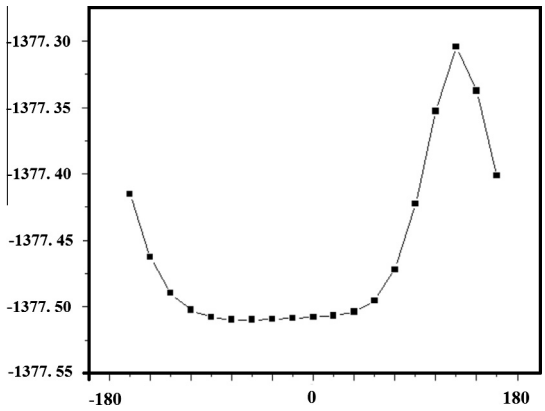

Fig. 5. Profile of potential energy scan for the torsion angle C_{30}—C_{17}—C_{12}—C_8.

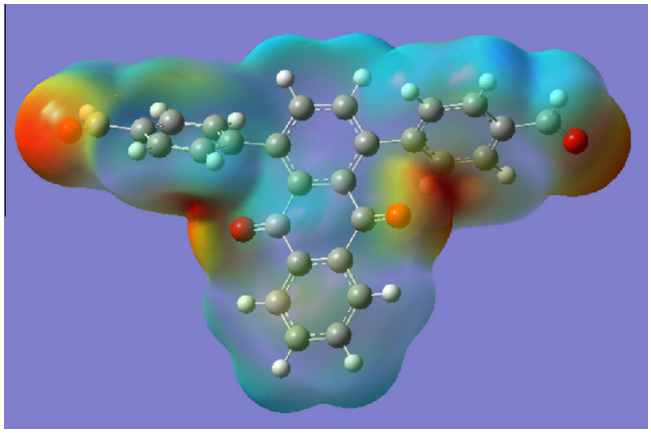

Fig. 6. Molecular electrostatic potential map calculated at B3LYP/6-31G* level.

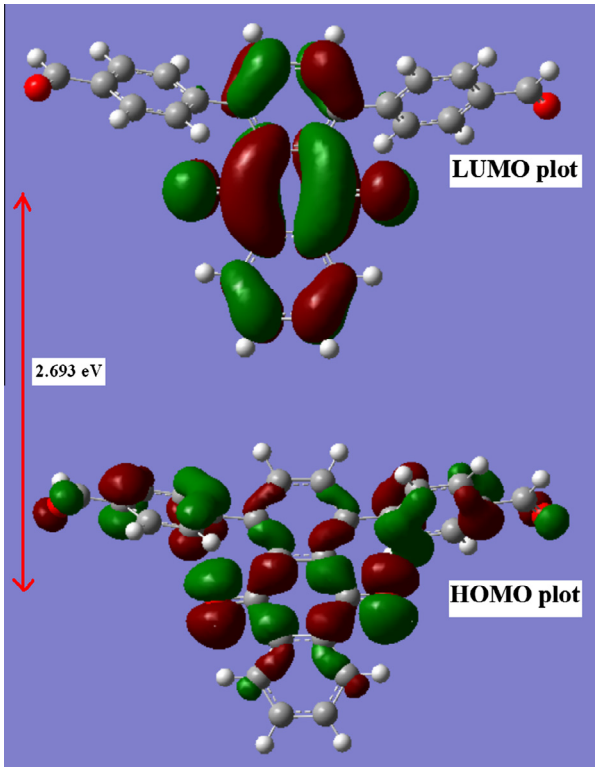

Fig. 7. HOMO and LUMO plots of 1,4-bis(4-formylphenyl)anthraquinone.

of a significant degree of ICT from the end-capping electron-donor groups to the efficient electron-acceptor groups through π-conjugated path. The strong charge transfer interaction through π-conjugated bridge results in substantial ground state donor–acceptor mixing and the appearance of a charge transfer band in the electronic absorption spectrum. Therefore, an ED transfer occurs from the more aromatic part of the π-conjugated system in the electron donor side to its electron-withdrawing part. The atomic orbital components of the frontier molecular orbitals are shown in Fig. 7. The HOMO–LUMO energy gap value is found to be 2.693 eV.

Conclusion

In this work, the vibrational spectral analysis was carried out using FT-IR and FT-Raman spectroscopy for 1,4-bis(4-formylphenyl)anthraquinone. The computations were performed at B3PW/6-31G* and B3LYP/6-31G* levels of theory to get the optimized geometry and vibrational wavenumbers of the normal modes of the title compound. The complete vibrational assignments of wavenumbers were made on the basis of potential energy distribution and using Gaussview software. The HOMO–LUMO analysis is used to determine the charge transfer within the molecule. The stability of the molecule arising from hyper-conjugative interaction and charge delocalization has been analyzed using NBO analysis. The calculated first hyperpolarizability of the title compound is 8.04×10^{-30} e.s.u, which is 61.85 times that of the standard NLO material urea. We conclude that the title compound is an attractive object for future studies of nonlinear optical properties. In 1,4-bis(4-formylphenyl)anthraquinone, the Mulliken atomic charge of the carbon atoms in the neighbourhood of C_7 and C_{10} become more positive, shows the direction of delocalization and shows that the natural atomic charges are more sensitive to the changes in the molecular structure than Mulliken's net charges.

Acknowledgement

RR thanks University Grants Commission, India, for a research fellowship and the authors are thankful to University of Antwerp for access to the university's CalcUA Supercomputer Cluster.

Appendix A. Supplementary material

Supplementary data associated with this article can be found, in the online version, at http://dx.doi.org/10.1016/j.saa.2014.04.085.

References

[1] H. Dave, L. Ledwani, Indian J. Nat. Prod. Resour. 3 (2012) 291–319.
[2] F.K. Li, C.K. Lai, W.T. Poon, A.Y.W. Chan, K.W. Chan, K.C. Tse, T.M. Chan, K.N. Lai, Nephrol. Dial. Transplant. 19 (7) (2004) 1916–1917.
[3] G.C. Yen, P.D. Duh, D.Y. Chuang, Food Chem. 70 (4) (2000) 437–441.
[4] N.H. Nam, G.Z. Jin, M.N. Tam, B.Z. Ahn, Arch. Pharmacal. Res. 22 (6) (1999) 592–607.
[5] Y. Baqi, C.E. Müller, Nat. Protoc. 5 (2010) 945–953.
[6] M.N. Tam, N.H. Nam, G.Z. Jin, G.Y. Song, B.Z. Ahn, Arch. Pharm. 333 (6) (2000) 189–194.
[7] D.S. Alves, L. Perez-Fons, A. Estepa, V. Micol, Biochem. Phramacol. 68 (2004) 549–561.
[8] R.J. Cox, Mol. Cryst. Liq. Cryst. 55 (1979) 1–32.
[9] Y.R. Shen, The Principles of Nonlinear Optics, Wiley, New York, 1984.
[10] P.V. Kolinsky, Opt. Eng. 31 (1992) 11676–11684.
[11] T. Joseph, H.T. Varghese, C.Y. Panicker, T. Thiemann, K. Viswanathan, C.V. Alsenoy, J. Mol. Struct. 1005 (2011) 17–24.
[12] D. Jacquemin, V. Wathelet, J. Preat, E.A. Perpete, Spectrochim. Acta 67A (2007) 334–341.
[13] C.R. Moylan, R.J. Twieg, V.Y. Lee, S.A. Swanson, K.M. Betterton, R.D. Miller, J. Am. Chem. Soc. 115 (1993) 12599–12600.
[14] S. Gilmour, R.A. Montgomery, S.R. Marder, L.T. Cheng, A.K.Y. Jen, Y. Cai, J.W. Perry, L.R. Dalton, Chem. Mater. 6 (1994) 1603–1604.

[15] T. Thiemann, Y. Tanaka, J. Iniesta, H.T. Varghese, C.Y. Panicker, J. Chem. Res. (2009) 732–736.
[16] O.A. Akrawi, A. Khan, T. Patonay, A. Villinger, P. Langer, Tetrahedron 69 (2013) 9013–9024.
[17] T. Thiemann, Y. Tanaka, J. Iniesta, Molecules 14 (2009) 1013–1031.
[18] Gaussian 09, Revision B.01, M.J. Frisch, G.W. Trucks, H.B. Schlegel, G.E. Scuseria, M.A. Robb, J.R. Cheeseman, G. Scalmani, V. Barone, B. Mennucci, G.A. Petersson, H. Nakatsuji, M. Caricato, X. Li, H.P. Hratchian, A.F. Izmaylov, J. Bloino, G. Zheng, J.L. Sonnenberg, M. Hada, M. Ehara, K. Toyota, R. Fukuda, J. Hasegawa, M. Ishida, T. Nakajima, Y. Honda, O. Kitao, H. Nakai, T. Vreven, J.A. Montgomery, J.E. Peralta, F. Ogliaro, M. Bearpark, J.J. Heyd, E. Brothers, K.N. Kudin, V.N. Staroverov, T. Keith, R. Kobayashi, J. Normand, K. Raghavachari, A. Rendell, J.C. Burant, S.S. Iyengar, J. Tomasi, M. Cossi, N. Rega, J.M. Millam, M. Klene, J.E. Knox, J.B. Cross, V. Bakken, C.Adamo, J. Jaramillo, R. Gomperts, R.E. Stratmann, O. Yazyev, A.J. Austin, R. Cammi, C. Pomelli, J.W. Ochterski, R.L. Martin, K. Morokuma, V.G. Zakrzewski, G.A. Voth, P. Salvador, J.J. Dannenberg, S. Dapprich, A.D. Daniels, O. Farkas, J.B. Foresman, J.V. Ortiz, J. Cioslowski, D.J. Fox, Gaussian Inc., Wallingford CT, 2010.
[19] J.B. Foresman, in: E. Frisch (Ed.), Exploring Chemistry with Electronic Structure Methods: A Guide to Using Gaussian, Pittsburg, PA, 1996.
[20] R. Dennington, T. Keith, J. Millam, Gaussview, Version 5, Semichem Inc., Shawnee Mission KS, 2009.
[21] J.M.L. Martin, C. Van Alsenoy, GAR2PED, A Program to Obtain a Potential Energy Distribution from a Gaussian Archive Record, University of Antwerp, Belgium, 2007.
[22] J. Mohan, Organic Spectroscopy – Principles and Applications, second ed., Narosa Publishing House, New Delhi, 2011. p. 30.
[23] V. Balachandran, G. Santhi, V. Karpagam, Spectrochim. Acta 106 (2013) 262–274.
[24] A. Nataraj, V. Balachandran, T. Karthick, J. Mol. Struct. 1031 (2013) 221–233.
[25] J. Coates, Encyclopedia of Analytical Chemistry: Interpretation of Infrared spectra, A Practical Approach (Ed. R. A. Meyers), John Wiley and Sons, Chichester, 2000.
[26] N.P.G. Roeges, A Guide to the Complete Interpretation of the Infrared Spectra of Organic Structures, Wiley, New York, 1994.
[27] G. Varsanyi, Assignments of Vibrational Spectra of Seven Hundred Benzene Derivatives, Wiley, New York, 1974.
[28] Y.S. Mary, H.T. Varghese, C.Y. Panicker, T. Ertan, I. Yildiz, O. Temiz-Arpaci, Spectrochim. Acta 71 (2) (2008) 566–571.
[29] A.R. Amjujakshan, V.S. Madhavan, H.T. Varghese, C.Y. Panicker, O. Temiz-Arpaci, B. Tekiner-Gulbas, I. Yildiz, Spectrochim. Acta 69A (2007) 782–788.
[30] S.E. Jorge-Villar, H.G.M. Edwards, J. Raman Spectrosc. 41 (2010) 63–67.
[31] A. Baran, B. Wrzosek, J. Bukowska, L.M. Proniewicz, M. Branska, J. Raman Spectrosc. 40 (2009) 436–441.
[32] S.Y. Lee, B.H. Boo, Bull. Korean Chem. Soc. 17 (1996) 754–759.
[33] S. Zilberg, Y. Hass, S. Shaik, J. Phys. Chem. 99 (1995) 16558–16565.
[34] D. Kafer, G. Witte, P. Cyganik, A. Terfort, C. Woll, J. Am. Chem. Soc. 128 (2006) 1723–1732.
[35] X. Wang, G. Valverde-Aguilar, M.N. Weaver, S.F. Neldon, J.I. Zink, J. Phys. Chem. A111 (2007) 5441–5447.
[36] J.V. Lockard, A.B. Ricks, D.T. Co, M.R. Wasielewski, Phys. Chem. Lett. 1 (2010) 215–218.
[37] S.A. Asher, Anal. Chem. 56 (1984) 720–724.
[38] A. Chandran, Y.S. Mary, H.T. Varghese, C.Y. Panicker, P. Pazdera, G. Rajendran, Spectrochim. Acta 79A (2011) 1584–1592.
[39] S.H. Brewer, A.M. Allen, S.E. Lappi, T.L. Chase, K.A. Briggman, C.B. Gorman, S. Franzen, Langmuir 20 (2004) 5512–5520.
[40] V. Krishnakumar, R.J. Xavier, Spectrochim. Acta 61 (2005) 1799–1809.
[41] E. Wnuk, P. Niedzialkowski, D. Trzybinski, T. Ossowski, Acta Cryst. E68 (2012) 2879.
[42] P. Niedzialkowski, D. Trzybinski, A. Sirkorski, T. Ossowski, Acta Cryst. E66 (2011) 33–34.
[43] J.E. Gautrot, P. Hodge, D. Cupertino, M. Helliwell, New J. Chem. 31 (2007) 1585–1593.
[44] N. Boonnak, S. Chantrapromma, H.K. Fun, S. Anjum, S. Ali, A.R. Rahman, C. Karalai, Acta Cryst. E61 (2005) 410–412.
[45] Z.S. Markovic, N.T. Manojlovic, S.R. Jeremic, M. Zivic, Hem. Ind. 67 (2013) 77–88.
[46] P. Sykes, A Guide book to mechanism in organic chemistry, ed.6, Pearson Education, India, New Delhi (2004).
[47] B.V.R. Murthy, Z. Kristallogr. 113 (1960) 445–465.
[48] L. Lunazzi, M. Mancinelli, A. Mazzanti, J. Org. Chem. 74 (2009) 1345–1348.
[49] C. Kitamura, H. Tsukuda, T. Kobayashi, H. Naito, X-ray Struct. Anal 26 (2010) 65–66. Online.
[50] W.Q. Fan, F.X. Chen, Acta Cryst. E68 (2012) 1831–1835.
[51] T. Suwunwong, S. Chantrapromma, C. Karalai, P. Pakdeevanich, H.K. Fun, Acta Cryst. E65 (2009) 420–421.
[52] J.deA. e Silva, C.Y. Vivas, A.J.F.N. Sorbal, M.R. Silva, Acta Cryst. E69 (2013) 705.
[53] D.F. Eaton, Science 25 (1991) 281–287.
[54] D.A. Kleinman, Phys. Rev. 126 (1962) 1977–1979.
[55] T. Joseph, H.T. Varghese, C.Y. Panicker, T. Thiemann, K. Viswanathan, C.V. Alsenoy, T.K. Manojkumar, Spectrochim. Acta 117 (2014) 413–421.
[56] M. Adant, L. Dupuis, L. Bredas, Int. J. Quantum. Chem. 56 (2004) 497–507.
[57] E.D. Glendening, A.E. Reed, J.E. Carpenter, F. Weinhold, NBO Version 3.1, Gaussian Inc., Pittsburgh, PA, 2003.
[58] J. Choo, S. Kim, H. Joo, Y. Kwon, J. Mol. Struct. (Theochem.) 587 (2002) 1–8.
[59] R.S. Mulliken, J. Chem. Phys. 23 (1955) 1833–1840.
[60] K. Wolinski, J.F. Hinton, P. Pulay, J. Am. Chem. Soc. 112 (1990) 8251–8260.
[61] E. Scrocco, J. Tomasi, Adv. Quantum. Chem. 103 (1978) 115–121.
[62] F.J. Luque, J.M. Lopez, M. Orozco, Theor. Chem. Acc. 103 (2000) 343–345.
[63] P. Politzer, J.S. Murray, in: D.L. Beveridge, R. Lavery (Eds.), Theoretical Biochemistry and Molecular Biophysics: A Comprehensive Survey. Protein, vol. 2, Adenine Press, Schenectady, New York, 1991.
[64] E. Scrocco, J. Tomasi, Curr. Chem. 7 (1973) 95–170.